



## Three-way junction skeleton biosensors based on aptamers, DNazymes, and DNA hybridization probes

Hamed Zahraee <sup>a, b, c</sup>, Zahra Khoshbin <sup>b, d, e</sup>, Fatemeh Mohammadi <sup>a, b, c</sup>,  
Mansour Mashreghi <sup>a, f, g</sup>, Khalil Abnous <sup>d, e, \*\*</sup>, Seyed Mohammad Taghdisi <sup>b, c, \*</sup>

<sup>a</sup> Department of Biology, Faculty of Science, Ferdowsi University of Mashhad, Mashhad, Iran

<sup>b</sup> Targeted Drug Delivery Research Center, Pharmaceutical Technology Institute, Mashhad University of Medical Sciences, Mashhad, Iran

<sup>c</sup> Department of Pharmaceutical Biotechnology, School of Pharmacy, Mashhad University of Medical Sciences, Mashhad, Iran

<sup>d</sup> Department of Medicinal Chemistry, School of Pharmacy, Mashhad University of Medical Sciences, Mashhad, Iran

<sup>e</sup> Pharmaceutical Research Center, Pharmaceutical Technology Institute, Mashhad University of Medical Sciences, Mashhad, Iran

<sup>f</sup> Industrial Biotechnology Research Group, Institute of Biotechnology, Ferdowsi University of Mashhad, Mashhad, Iran

<sup>g</sup> Nano Research Center, Ferdowsi University of Mashhad, Mashhad, Iran



### ARTICLE INFO

#### Article history:

Received 20 January 2023

Received in revised form

23 June 2023

Accepted 24 June 2023

Available online 26 June 2023

#### Keywords:

DNA origami

Three-way junction

Signal amplification

Multifunctional

Nanostructure

Aptasensor

### ABSTRACT

Nucleic acids can be used as building blocks for highly regular and complex structures at the nanoscale due to their inherent self-assembly and programmability resulting from intra- and inter-molecular interactions. Three-way junctions (TWJs) structure is recognized as the smallest type of junction in nucleic acids. To form TWJ nanostructures, three DNA or RNA strands with complementary segments at each end are hybridized and form a Y-shaped structure. TWJ skeletons, having three independent arms, provide multifunctional sites for beneficial amplification, recognition, and signaling purposes in specific biomolecular nanoarchitecture. In this study, we represent the superiority aspects on the achievements of the biosensors with the cooperation of DNA/RNA TWJ nanoskeletons for monitoring different targets. Moreover, some discussions are declared to achieve a perspective for developing promising TWJ-based aptasensors in the future. This in-depth study can open a constructive way for commercializing and miniaturizing TWJ-tuned aptasensors as user-friendly lab-on-chip sensing devices.

© 2023 Elsevier B.V. All rights reserved.

### 1. Introduction

Aptamers are oligonucleotide sequences mostly made of DNA or RNA with a length of 20–100 nucleotides with high binding potential to different types of molecules, proteins, ions, and cells [1–3]. The high specificity of aptamers for target molecules is due to their unique three-dimensional structure, which allows them to specifically bind to their target molecules through weak interactions such as hydrogen bonding, electrostatic interactions, van der Waals forces, and hydrophobic interactions with high affinity [4–7]. Aptamers cause of the many advantages they have over antibodies and other biological receptors, including selectivity in-

vitro, stability against heat and pH, refolding to the original conformation after removing the denaturing agents, non-immunogenicity, and simple synthesis, making them potential diagnostic parts for design and engineering of biosensors [8–13].

DNA molecules as excellent building blocks in creating nanosized supramolecular architectures in the form of self-assembly, as a widely used structure, have attracted great attention in nanoscale assemblies, targeted drug delivery, and biosensors [14–16]. From the early 1960s, carried out extensive research into delivery methods and binding modes between small molecules and DNA, as a result of which binding modes of intercalation, groove binding, and DNA metalation were identified [17]. The capability of DNA to interact with small molecules is very important because, in addition to its ability to act as a carrier for drug delivery, it also provides the possibility of diagnostic applications in the environment, medicine, and food safety as a promising component of biosensors [18–22]. The formation of DNA supramolecular structures, including DNA origami structures and junctions based on the regulatory self-assembly feature of DNA was introduced by Seeman

\* Corresponding author. Targeted Drug Delivery Research Center, Pharmaceutical Technology Institute, Mashhad University of Medical Sciences, Mashhad, Iran.

\*\* Corresponding author. Department of Medicinal Chemistry, School of Pharmacy, Mashhad University of Medical Sciences, Mashhad, Iran.

E-mail addresses: [abnouskh@mums.ac.ir](mailto:abnouskh@mums.ac.ir) (K. Abnous), [taghdisihm@mums.ac.ir](mailto:taghdisihm@mums.ac.ir) (S.M. Taghdisi).

et al. in the early 1980s [23,24].

Junctions are formed by at least three DNA helices that meet at the same point [25,26]. DNA three-way junctions (TWJs) are one of the unique and simplest supramolecular and branched DNA structures because of their conformational versatility and stability, which are formed through sequence-dependent self-assembly of three DNA arms [27–29]. TWJ structures are formed through Watson-Crick base pairing between two of the three oligonucleotides at a central branch point in the form of three arms of double-helix [30,31]. These DNA-based nanostructures have high stability. For example, the TWJ structures synthesized by Li et al. [32] were stable for 30 days at low temperature (about 4 °C) without any degradation. Arms in TWJs provide functional flexibility and perform functions such as recognizable sites or placement of a signal reporter at the central branch point [33–36]. Typically, two strategies are used for the synthesis of TWJs, as shown in Fig. 1; there is no difference in the results between the two mentioned approaches. (1) Stepwise synthesis: In this method, complementary segments on two single strands form an arm of a double helix. Then, the other two arms of TWJ are formed by the third single strand, which complements the two unconnected parts of the previous strands. (2) All-in-one synthesis: In this approach, three strands with equal molar concentrations are combined simultaneously, leading to the formation of TWJ structures [32].

TWJ structures exhibit the structural characteristics of coaxial stacking [37]. Compared to duplexes, their formation requires mechanisms for neutralization and hydration due to the presence of negative charges from the phosphate groups around the junction point [38,39]. In a study by Muhuri et al. [40] on the role of water molecules and  $Mg^{2+}$  cations on the thermodynamics and three-dimensional structure of TWJs, it was found that a concentration of 5 mM  $Mg^{2+}$  ions stabilizes TWJ structures. This results in a significant increase in the free energy changes ( $-\Delta G$  37°) for the two possible conformations that can be formed by TWJs with two unpaired thymine bases at the junction (A/B and A/C stacked conformers) from 3.7 to 3.0 kcal/mol to 5.6 and 3.7 kcal/mol, respectively. Additionally, hydration plays an important role during the formation of TWJs. The dehydration of the junction point in TWJs facilitates their formation in environments where hydration is less favorable, such as intracellular conditions, compared to double-stranded DNA. As described by Yang et al. [41], catalyzing the formation of TWJ motifs using a primer DNA strand can be

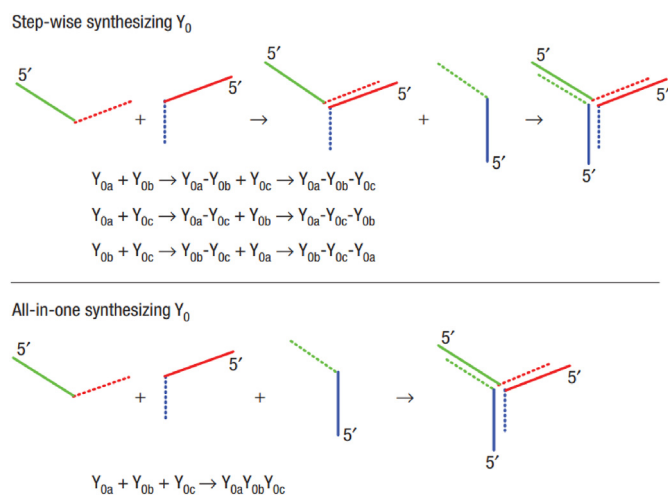
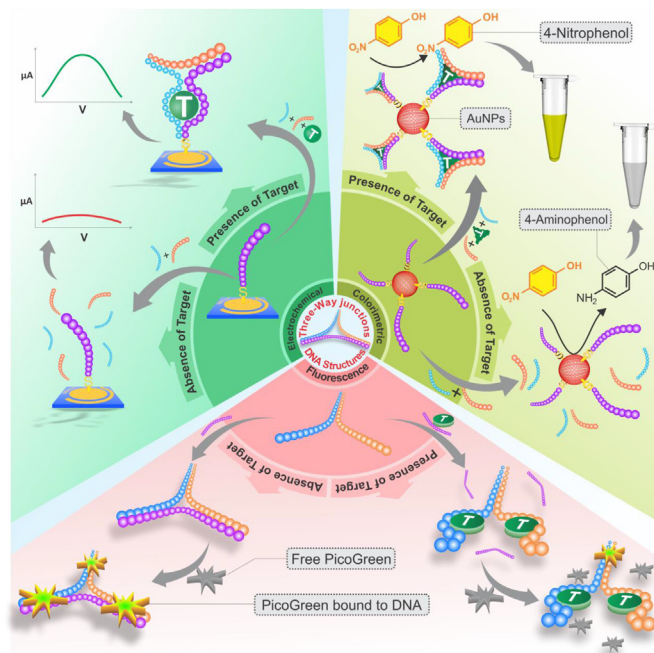


**Fig. 1.** Two strategies of TWJ synthesis. The strands  $Y_{0a}$ ,  $Y_{0b}$ , and  $Y_{0c}$  refer to each arm of the TWJ structure. Reproduced from the literature [32] with permission from Springer Nature.

achieved through a competitive hybridization cascade. Also, TWJ nanostructures can be synthesized as programmable scaffolds using a repeated primer strand recycling cycle. These strategies for the assembly and synthesis of TWJs can be easily generalized to construct other types of junctions and branched DNAs [42–44]. Branched DNA nanoarchitectures have high potential in nanotechnology and biomedicine due to their morphology and size [45–48]. TWJs that respond to target ligands are used as building blocks for designing DNA nanoarchitectures with variable structures, providing a beneficial way to design biosensors with new capabilities [49–52]. For example, Zhang et al. [53] engineered a new multi-functional sensor platform based on DNA-TWJ with three functional parts for the simultaneous detection of three different types of targets (DNA, thrombin, and ATP) by investigating independent electrochemical, fluorescent, and colorimetric signal outputs. The development of an efficient biosensor by Ma et al. [54] for the detection of  $Hg^{2+}$  metal ion using a DNA-TWJ structure with the lowest detection limit (LOD = 0.04 pM) to date and excellent selectivity has garnered increasing attention for extending TWJ-mediated ion sensing methods. In another study by Bian et al. [55], DNA nanotweezers with TWJ-like structures were used as DNA nanoswitches to achieve enzyme-free biosensor for the ultrasensitive detection of PML/RAR $\alpha$  fusion gene as an important biomarker in leukemia diagnosis. This detection system with an ultralow detection limit of 0.125 fM demonstrated the potential of TWJ structures in DNA nanodevices as a promising tool for ultrasensitive nucleic acid detection. TWJ nanostructures can also be a part of DNA nanomaterials, such as DNA tetrahedral frameworks (DTFs) as a DNA programmed structure, which provide a platform for ultrasensitive and simultaneous detection of exosomal miRNAs for early detection of non-small cell lung cancer (NSCLC) with a wide dynamic range of 2 fM–20 nM and an excellent detection limit of 1.68 fM [56]. In this review, we have focused on biosensors based on the DNA/RNA-TWJ structure; and a variety of electrochemical, fluorescence, colorimetric, and surface-enhanced Raman spectroscopy methods based on TWJ nanoarchitectures for detecting



**Scheme 1.** Schematic of aptasensors based on TWJ nanoskeleton classified by output signals.

biomarkers, small molecules, genes, microbial pathogens, and cancer cells have been discussed in detail (Scheme 1).

## 2. Aptasensors based on TWJ nanostructure for biomarkers detection

In recent years, researchers have made significant progress in the development of ultrasensitive detection assays by electrochemical, fluorescence, colorimetric, and surface-enhanced Raman spectroscopy (SERS) aptasensors that use TWJ nanoskeleton to monitor biomarkers. Jiang et al. [57] developed an ultrasensitive biosensor based on an enzyme-free amplification process for the electrochemical detection of miRNA-21 as a model biomarker target. The sensing principle is shown in Fig. 2A. The biosensor included a thiol-attached capture probe (CP), a hybrid of L strand with methylene blue-labeled S strand (MB-S), and three hairpin probes (H0, H1, and H2). The L strand possessed some nucleotides more than the S and CP strands to achieve the high stability of the L/S-MB duplex. The surface of an Au electrode was modified by the CP sequences through Au-S interaction. The H0 strand contained a loop segment attached to the specific DNA sequence toward the miRNA-21. The H1 and H2 strands with some complementary segments possessed a dual-binding susceptibility of interlocking to each other and the H0 strand. In the presence of the miRNA-21, it was hybridized with the stem-locking part of the H0 strand. The expanded H0 strand with the free tails initiated the catalyzed hairpin assembly process by involving the H1 and H2 strands. The numerous copies of the H1/H2 duplexes were achieved by continuing the catalyzed hairpin amplification process. With adding the L/S-MB duplex, a TWJ structure between the free tail of the H1/H2 duplex and L strand was formed that released the MB-S sequence. The free MB-S strand was complexed with the CP strand on the electrode surface which enhanced the electrochemical signal. In the lack of the miRNA-21, no free S strand was generated for hybridization to the CP, obtaining a negligible output signal. The biosensor possessed high sensitivity, and universality for diverse targets by replacing the H0 strand, simple operation, and enzyme-free mechanism. Also, Hu et al. [58] constructed a simple electrochemical biosensor for monitoring miRNA-21 by using a distinguishable locked nucleic acid (LNA) probe owning greater thermal stability, less background noise, and higher binding affinity than normal DNA strands. The capture sequence with three

LNA segments was immobilized on the Au electrode covalently. With adding miRNA-21, the TWJ structure was formed with the aid of the MB-attached signal probe strand. So, the MB molecule was placed near the electrode surface, increasing the current response. Moreover, tris-(2-carboxyethyl) phosphine hydrochloride (TCEP) as a chemical reductant was added that chemically reduced the electroactive MB near the electrode surface. The reduction process was repeated through the redox cycling process that amplified the electrochemical response. In comparison with the routine signal amplification approaches, the developed strategy possessed no expensive and sensitive enzymes and intricate nanomatters. Consequently, it is potent for disease diagnostics and clinical analysis. In comparison, Hou et al. [59] fabricated a tag-free electrochemiluminescence (ECL) biosensor to monitor miRNA-21 by using an LNA probe and a complex of perylenetetracarboxylic acid (PTCA), graphite-like carbon nitride ( $g\text{-C}_3\text{N}_4$ ), graphene quantum dots (GQDs), and gold nanoparticles (AuNPs) as a luminophore.  $g\text{-C}_3\text{N}_4$  nanosheet acted as a nanocarrier. GQDs and PTCA were immobilized on the  $g\text{-C}_3\text{N}_4$  surface to provide a great number of  $\text{-COOH}$  groups. AuNPs were applied to enhance the conductivity. The PTCA@ $g\text{-C}_3\text{N}_4$ @GQDs@AuNPs composite provided high efficiency and stable ECL emission through the synergistic effect with  $\text{Na}_2\text{S}_2\text{O}_8$  co-reactant. A glassy carbon electrode (GCE) was treated by the PTCA@ $g\text{-C}_3\text{N}_4$ @GQDs@AuNPs composite. Then, the CP sequence was fixed on the GCE surface by the carbodiimide-aided wet chemistry method. In the presence of the target, a TWJ structure was formed including the capture probe, LNA strand, and miRNA that blocked the contact of the  $\text{Na}_2\text{S}_2\text{O}_8$  co-reactant with the luminescent agent on the GCE surface. So, the ECL response decreased significantly. With the properties of a wide detection range and great sensitivity, the biosensing assay is efficient for RNA detection in clinical samples. In another study conducted on other miRNA models, Chang et al. [60] constructed an ultrasensitive electrochemical aptasensor to monitor miRNA-182-5p by applying a DNA TWJ with recognition elements in hairpin stems. The target presence opened the hairpin parts and formed an annular structure of the DNA walker through interacting with three recognition segments. The produced DNA walker opened the ferrocene (Fc)-tagged hairpin strand, attached on the GCE surface, achieving double-stranded DNAs. The double strand was cleaved by Nt. BstNBI endonuclease that released the Fc-labeled fragment from the electrode surface. Besides, a great number of DNA walkers were

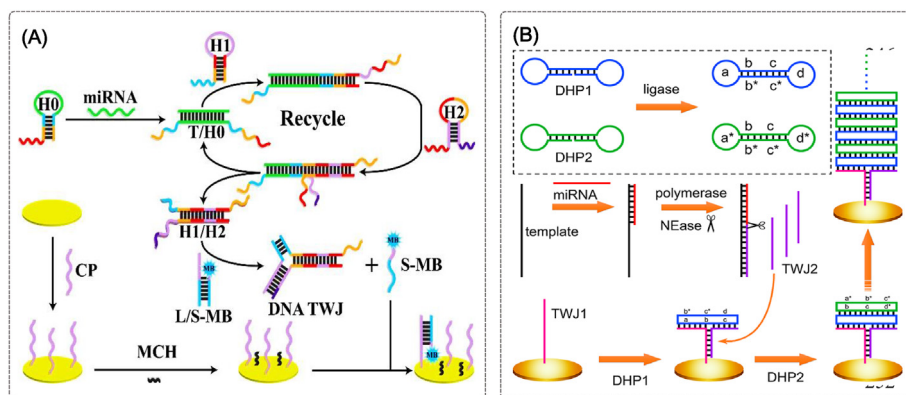


**Fig. 2.** (A) Schematic illustration of the electrochemical method for sensing miRNA. The presence of miRNA proceeded the enzyme-free amplification process through hybridizing to the H0 strand and forming numerous H1/H2 duplexes by the hairpin assembly process. A TWJ structure was formed between the free tail of the duplex and the L strand of the L/S-MB complex. So, the released MB-S strand interacted with the CP strand on the electrode surface which increased the output signal. Represented by permission from Ref. [57], Royal Society of Chemistry. (B) Schematic design of the electrochemical biosensing method for miRNA. The hybridization of the miRNA target with the DNA template was completed through the catalytic activity of the polymerase enzyme. After the duplex was cleaved by NEase, a large number of TWJ2 strands were produced, which hybridized with the immobilized TWJ1 strand on the electrode surface. Subsequently, a ladder containing the DHP1 and DHP2 strands was formed through DHCR on the electrode surface, leading to the development of a TWJ biosensor capable of monitoring miRNA. Represented by permission from Ref. [61], American Chemical Society.

released for participating in another amplification cycle. Consequently, the output signal decreased significantly. The developed detection assay possessed the great stability during 20 days, making it efficient for clinical application. In addition to the electrochemical aptasensor developed by Chang et al. [60] for the miRNA-182-5p detection, Miao and Tang [61] developed an ultra-sensitive TWJ aptasensor to detect exosomal miRNA as a noninvasive cancer biomarker by combining dumbbell hybridization chain reaction (DHCR) and strand displacement amplification (SDA). As indicated in Fig. 2B, the miRNA formed a DNA duplex by partial hybridization with a DNA template. It was extended to a complete duplex by the catalytic activity of the polymerase enzyme. Then, a great number of the TWJ2 single strands were obtained by NEase. The TWJ2 strand partially interacted with the immobilized TWJ1 on the electrode surface. For the DHCR process on the electrode surface, two probes were applied: DHP1, containing the segments a, b, c, d, b\*, and c\*; and DHP2, containing a\*, b\*, c\*, d\*, b, and c. The dumbbell-shaped structure was formed through the hybridization of the complementary parts of DHP1 and DHP2. The closed state of the phosphorylated DHP strands was obtained by the activity of T4 DNA ligase, attaining the sufficiently stable dumbbell-shaped DNA structure. The complete TWJ structure was formed through the hybridization of the TWJ1, TWJ2, and DHP1. The single part of DHP1 provided the anchorage for stacking the dumbbell-shaped DHP2 strand. Similarly, the free parts of DHP2 achieved a new hybridization with another DHP1. The hybridization reaction was recycled, leading to the assembly of DHP1 and DHP2 strands on the electrode surface. As a result, the electrochemical signal increased, indicating the presence of the miRNA target. With the highest sensitivity, the sensing method is potent for miRNA analysis in clinical cancer samples.

Many miRNAs (especially miRNA-21, miRNA-27a, and miRNA-375) with high expression in breast cancer play a key role in the development and progression of the disease. So, identifying these factors helps a lot in the diagnosis and treatment of cancer [62–64]. Therefore, Wang et al. [65] represented a new detection method for three cancer-related serum exosomal miRNAs (miRNA-21, miRNA-27a, and miRNA-375) based on TWJ formation. As indicated in

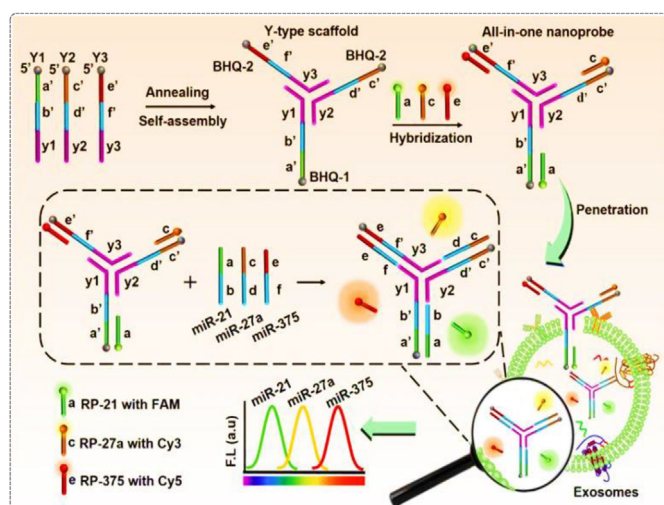


**Fig. 3.** Steps of formation and function of multiplex biosensor in exosome of human serum with breast cancer. The probe of each target miRNA (miR-21, miR-27a, and miR-37) was labeled with a specific fluorescent dye (FAM, Cy3, and Cy5) and added to the system. With the entry of the sensing system into the exosome, a TWJ structure was obtained in the presence of the target miRNAs, which caused the reporter to separate from its quenchers and therefore, the release of the various fluorescent signals. Reproduced with permission from Ref. [65], Elsevier.

Fig. 3, the designed biosensor possessed three identification sequences (Y1, Y2, and Y3) modified by quenchers (BHQ1, BHQ2, and BHQ3 respectively). Also, three reporter sequences were labeled by the different fluorescent dyes (FAM, Cy3, and Cy5) and added to the identification sequences. The multicolor biosensor was hybridized with three different complementary miRNAs that formed TWJ structures. So, the reporter sequence was released and, as a result, the different fluorescent signals were produced. The proposed biosensor is non-invasive, cheap, and easy with good stability and reproducibility. Hence, it has a high potential for clinical diagnosis of various diseases, including breast cancer through the simultaneous detection of different miRNAs.

Another miRNA-based biomarker is let-7a, which is a member of the first group of miRNAs discovered (let-7). Let-7a miRNA is involved in several biological processes, such as cell proliferation, apoptosis, development, and migration of cancer [66–68]. For example, let-7a miRNA can act as a tumor suppressor by targeting oncogenes such as RAS and HMGA2 in laryngeal and breast cancers, respectively [69,70]. For this reason, Zhang et al. [71] designed a bipedal-unequivalent three-dimensional DNA walker based on a DNA TWJ switch (DTWJS) for the bioassay of miRNA let-7a as a prognostic biomarker in various biological fluids, which can be used as a powerful analytical tool in future medical diagnosis. As shown in Fig. 4, the intended aptasensor consisted of AuNPs modified by two long strands with nearly complementary sequences called bipedal walking strand (B-UWS) and a shorter strand containing target recognition motif sequence called blocker. Clamps (H1 and H2) labeled by FAM acted as the pathway strands and complementary of the hairpins (H3 and H4) that formed the fuel strands of the sensing platform. The FAM marker was kept off

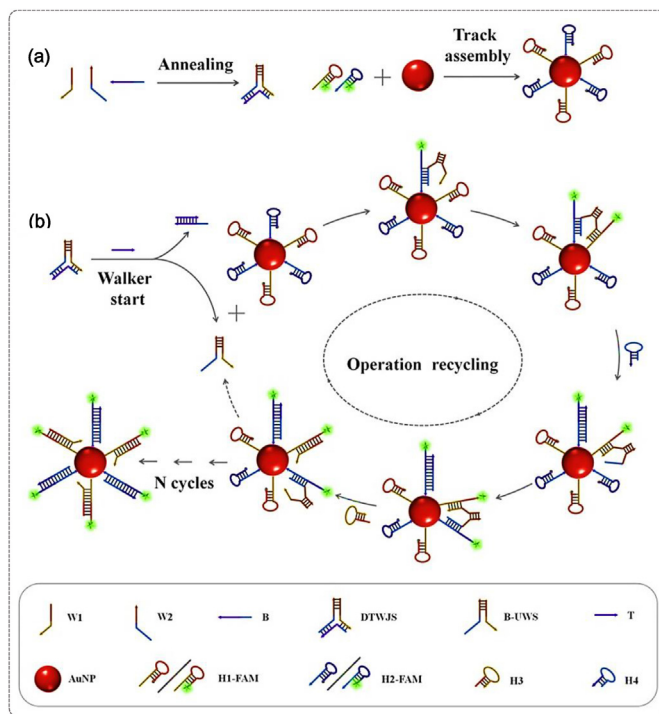


**Fig. 4.** Steps of the formation and operation of 3D Walker DNA aptasensor. (a) The Three-way DNA binding switch consisted of three parts, including two long strands with nearly complementary sequences (W1 and W2) and a short strand (B) mounted on AuNPs. (b) The target bound to the B strand caused the separation of B-UWS. The FAM-modified H1 and H2 were hybridized with H3 and H4 hairpins, respectively, and created a walker for the B-UWS movement. B-UWS continued to move sequentially with the help of a walker through hybridization with the other strands, which increased the fluorescence signal. Reprinted by permission from Ref. [71], Elsevier.

by AuNPs, but after binding the let-7a to the blocking strand, the B-UWS was dissociated and hybridized with H1 and H2 through the strand displacement reaction, and then, the H1 and H2 strands were connected to the H3 and H4 that formed the duplexes (H1–H3/H2–H4) as the aptasensor walkers. In this way, the successive hybridization of B-UWS with the string of other pathways led to the accumulation of FAM molecules and increased fluorescence signal. In the absence of the let-7a, B-UWS was trapped by DTWJS, and the walker action was not initiated. The stable performance potential of this platform for the detection of let-7a was twice that of a unipedal or the bipedal equivalent walker. Due to the difference in the DNA sequence of the two inequivalent pedals, they had the different affinities for B-UWS. This led to improved performance stability of the sensing system, increased adjustability, and reduced simultaneous stagnation of the strands for walking.

On the other hand, Cui et al. [72] designed a novel self-assembly DNA machine (ECDM) based on the self-assembly of copper nanoparticles (CuNPs) and TWJ structure for ultrasensitive detection miRNA-153 in serum for the diagnosis of Parkinson's disease. ECDM consisted of three important components including the TWJ hairpin probe, TWJ helper probe (with cutting site at the 3' end), and miRNA-153, which were partially complementary to each other. With the addition of miRNA-153, a stable structure was formed, and the cut site for the Nt.BspQI enzyme appeared on the double-stranded DNA. By cutting Nt.BspQI, the 3' end of the helper probes was extended by TDT enzyme that created poly-T. Again, this point was cut by Nt.BspQI and many single-chain poly-T were produced during several cycles. Copper ions ( $\text{Cu}^{2+}$ ) were used with Poly-T as a template to synthesize CuNPs, and self-assembly of the CuNPs was achieved. The higher the target concentration, the more CuNPs were produced. As a result, a stronger fluorescent signal was attained, which led to the target detection with femtomolar sensitivity. This easy, low-cost, and high-sensitive strategy can detect miRNA in minutes at room temperature (28–31 °C) and has great prospects for helping to diagnose various diseases (e.g., Parkinson's), and the prognosis of tumors.

As another advantage of TWJs, these structures are able to control monofunctionalization of AuNPs with RNA molecules for developing RNA nanotechnology applications. In this regard, Lee et al. [73] developed a biosensor based on monoconjugation of AuNPs with RNA TWJ to detect miRNA-155 using presented electrochemical SERS (EC-SERS). As shown in Fig. 5A, AuNPs were coated by streptavidin and were immobilized on a substrate of indium tin oxide (ITO) and AuNP as the electrode modifier. Each AuNP was conjugated to a copy of RNA TWJ bundle, so that one strand of RNA TWJ was modified by Sephadex G100 aptamer, and another strand was treated by a biotin molecule. In addition, one end of the third strand was modified by a thiol group to attach the monovalent TWJ/AuNP to the substrate surface, and its other end was modified by methylene blue as a Raman and redox reporter. Interaction of the specific aptamer with miRNA-155 resulted in proximity of methylene blue to AuNP and therefore, a dramatic increase in the SERS signal. Formation of a robust  $\lambda$ -shaped RNA chip (resulting from RNA flexibility and stability of RNA/RNA hybrid), applying constant optimal potential, use of monoconjugate instead of multifunctional AuNPs (with reduced inhibitory effects and creation of a suitable surface for effective methylene blue collision), and presence of a ring at the junction (by improving the structural key) led to a 7-fold signal amplification. The proposed method can provide new insights into RNA nanotechnology and biosensors for nucleic acid detection.

The rolling circle amplification (RCA) technique is an efficient enzymatic approach for the isothermal amplification of nucleic acid in a short time [74,75], which in combination with TWJ nanostructures in biosensor systems can be an ultra-sensitive, rapid, and

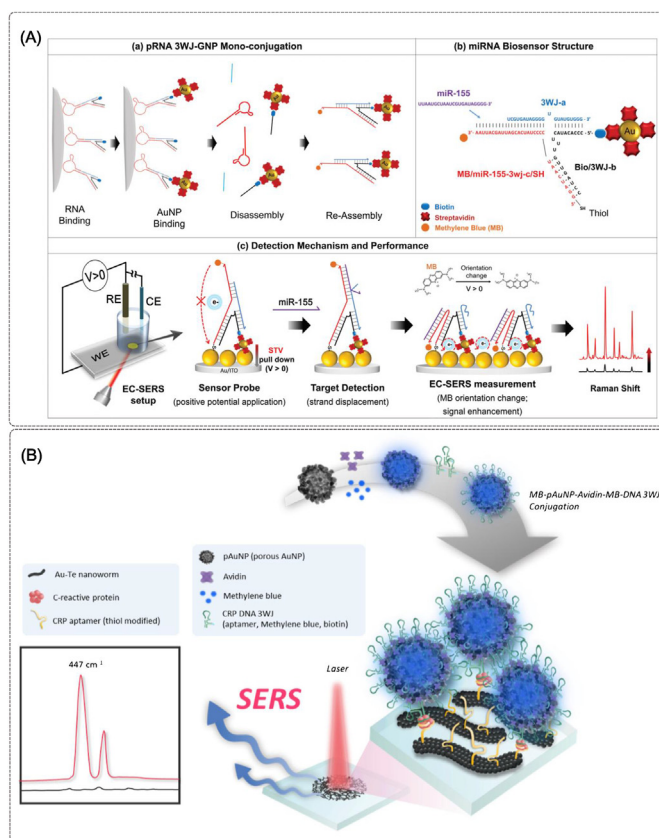


**Fig. 5.** (A) Illustrations of the biosensor structure and its diagnostic mechanism for miRNA-155. (a) First, a copy of modified RNA TWJ was fixed and attached to a single AuNP. Then, it was separated into three parts using buffer: TWJ-a, STV/AuNP-Bio/TWJ-b, and SEPapt/TWJ-c. The last fragment was modified by thiol and methylene blue before being reassembled. (b) The structure and sequence of RNA TWJ, which formed the miRNA-155 biosensor. (c) The interaction of miRNA-155 with the aptamer led to changes in the aptamer structure and resulted in the displacement of the TWJ-c strand, bringing methylene blue closer to the AuNP and ITO substrate, and increasing the SERS signals. Reprinted by permission from Ref. [73], Wiley. (B) Overview of the structure and function of the CRP biosensor. The CRP aptamer was attached to the Au-Te by covalent binding. Avidin and methylene blue were attached to pAuNPs by electrostatic attraction. Three modified nucleic acid strands were assembled, and a DNA TWJ was formed. In the presence of the different concentrations of CRP, the Raman signals, amplified by methylene blue, can be detected and measured. Reprinted by permission from Ref. [86], Springer.

accurate platform for real-time target monitoring in clinical research [76]. Identifying the expression overlap of different miRNAs is important for the diagnosis and treatment of different cancers. Therefore, TWJ constructs can be used as ideal elements alongside enzymatic systems such as clustered regularly interspaced short palindromic repeats (CRISPR) and RCA to potentially detect multiple miRNAs simultaneously. Qu et al. [77] designed a fluorescent platform for the simultaneous detection of miRNA-21 and miRNA-141, consisting of a TWJ probe with three DNA sequences (Y1, Y2, and Y3),  $\text{Fe}^{\text{II}}_4\text{L}_4$  tetrahedron as a quencher, and CRISPR-assisted RCA system. Both ends of the Y3 sequence were labeled by FAM and Cy3 fluorescent groups, and they were quenched by hybridizing with the BHQ-modified Y1 and Y2 complementary strands.  $\text{Fe}^{\text{II}}_4\text{L}_4$  tetrahedron also possessed a significant role in the fluorescence quenching of the included FAM dye in the DNA TWJ structures. If miRNA-21 and miRNA-141 were present at the same time, they could be hybridized with the Y1 and Y2 strands that released Y3. The released Y3 was entered into the RCA process, initiated by forming a closed loop structure of Y3 under the activity of the T4 ligase enzyme. The produced ssDNA from PCR process

could activate the *trans*-cleavage of CRISPR/Cas12a, which led to digestion of the reporter probe containing a fluorescent group (CY5) and quencher (BHQ2). So, a fluorescent signal was achieved significantly. This platform maintains its stability at 60°C and can save 5 h of time compared to the normal TWJ-based sensing platform, which is a suitable option in the field of diagnosis and treatment.

Circulating tumor DNA (ctDNA) is a highly promising non-invasive biomarker for monitoring cancer status [78–80]. In recent years, researchers have been exploring innovative approaches to develop highly efficient and sensitive electrochemical biosensors for ctDNA [81–84]. One such approach is the developed electrochemical aptasensor by Chai and Miao [85] that used TWJ and triangular prism (TP) arrangements of DNA strands with superior efficiency for molecular recognition of the biomarker ctDNA. This aptasensor was designed by five strands to form a TP nanostructure as a scaffold for ctDNA. With the aid of four thiol-modified TP strands, the rectangle bottom of the TP nanostructure was formed on the Au electrode surface. The single strands on the top of the TP nanostructure provided the region for the creation of the TWJ structure by involving the products of the isothermal amplification approach initiated by the ctDNA target. A template strand was designed with some complementary segments of the ctDNA. So, a partial DNA duplex was formed by the hybridization of the ctDNA and DNA template. The ctDNA was extended by the polymerase activity that completed the DNA duplex. Since the DNA duplex possessed a nicking site for the endonuclease, its cut was done in the presence of the enzyme. The polymerization reaction cycle was repeated that produced a great number of TWJ1 strands. With the aid of the TWJ2 probe tagged by ferrocene (Fc), the complete TWJ structure was formed on the top of the TP nanostructure, generating a potent generate electrochemical response. This electrochemical biosensor with ultrahigh sensitivity is efficient for clinical applications.

Kim et al. [86] presented an ultrasensitive biosensor using multifunctional DNA TWJ for the detection of C-reactive protein (CRP) based on SERS technique. To fabricate the sensing system, Au–Te nanoworm structures were fixed on an ITO plate, and then, thiol-modified CRP aptamer was anchored on the structures (Fig. 5B). Each DNA strand of the multifunctional TWJ was modified so that the first arm contained the CRP aptamer, the second arm was bound to methylene blue to generate the Raman signal, and the other arm was labeled with biotin to bind to the surface of porous gold nanoplates (pAuNPs). Then, the TWJ structures were conjugated to the pAuNPs, and by their interacting with the CRP, the signal intensity increased. Since pAuNPs possessed a large surface and combined with methylene blue, they strengthened the signal. The study revealed that DNA TWJs with their distinct structure can simultaneously perform the triple function of signal reporter, diagnostic component, and binding agent to nanoparticles. The proposed strategy can be inspiring with high potential in the development of diagnostic tools.

Despite the implementation of different strategies and output signals, these approaches demonstrate the versatility and adaptability of TWJ nanostructures in detecting a variety of biomarkers, such as miRNA-21, miRNA-182–5p, miRNA-141, let-7a miRNA, miRNA-153, miRNA-27a, miRNA-375, ctDNA, and CRP, which makes them promising candidates for clinical applications.

### 3. Aptasensors based on TWJ nanostructure for small molecules detection

Small molecules are some of the most critical organic compounds for biological functions as substrates or products that have a relatively low molecular weight (less than 900Da). They can be

either naturally occurring or synthetic and have a wide range of applications, including as drugs, hormones, pesticides, and antibiotics. The unique structures of TWJs allow for the precise control of the distance between the recognition and signal transduction elements, enabling highly sensitive and selective detection. By incorporating DNzyme and fluorescent probes, and dyes (such as N-methyl mesoporphyrin IX (NMM), Thioflavin T (ThT), and Pico-Green (PG)) in the TWJ-based aptasensors, the sensitivity and specificity of the sensors increase, and make them capable of detecting small molecules at very low concentrations. In a study by Fan et al. [87], a novel fluorescent aptasensor was designed for the detection of the pesticide isocarbophos, as shown in Fig. 6A. The aptasensor consisted of the AT-rich DNA TWJ structure (TWJ-1, TWJ-2, and TWJ-3), copper nanoparticles (CuNPs) fluorescent probe, AP-1 aptamer for the target binding, and magnetic Fe<sub>3</sub>O<sub>4</sub>@GO as the ssDNA adsorbent. TWJ-1 was partially complementary to AP-1, but when there was the target in the sample, the AP-1 interacted with the target, which released TWJ-1. Subsequently, it was hybridized with the TWJ-2 and TWJ-3 strands that formed a TWJ structure, which could not be absorbed on Fe<sub>3</sub>O<sub>4</sub>@GO due to its blunt terminals. By adding ascorbic acid (AA) and copper element (Cu<sup>2+</sup>) into the supernatant solution, a strong fluorescent signal was achieved through the formation of CuNPs on the TWJ

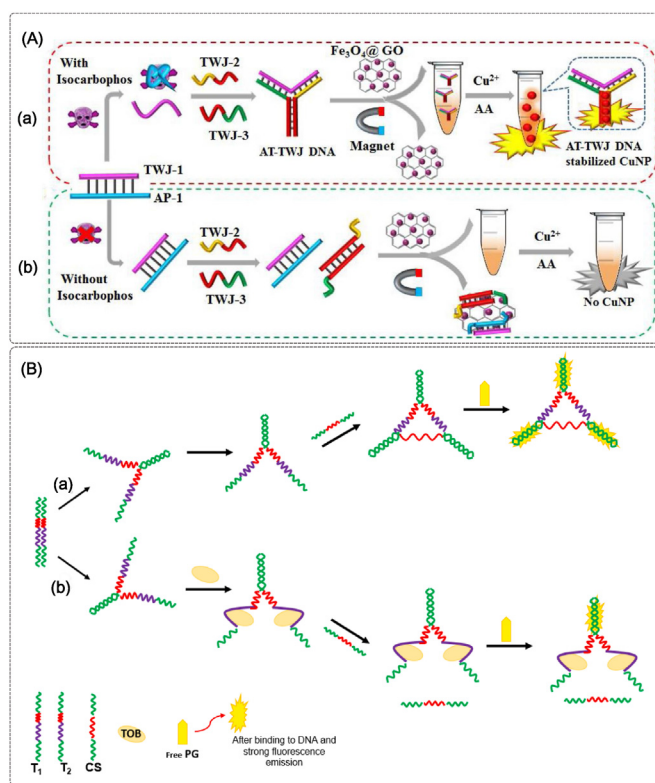


**Fig. 6.** (A) Schematic diagram of the fluorescent aptasensor for monitoring isocarbophos. With adding TWJ2 and TWJ3, a TWJ structure was formed that provided sites for the production of CuNPs, leading to an increase in fluorescence signal. In the absence of isocarbophos, the duplexes were adsorbed on Fe<sub>3</sub>O<sub>4</sub>/GO by their open tails. After magnetic separation, there was no DNA strand as the scaffold for the formation of CuNPs, which reduced the output signal. Represented by permission from Ref. [87], Elsevier. (B) TWJ-based aptasensor for tobramycin detection. (a) In the absence of tobramycin, three T1, T2, and CS strands were hybridized, which formed three dsDNA regions. Thus, PG was excited by binding to these regions which led to fluorescence emission. (b) Tobramycin interacted with the hybridized T1 and T2 and the resulting spatial structure prevented the hybridization of the CS strand. Hence, there was only one dsDNA region for the PG anchoring, resulting in a very weak fluorescence emission. Reprinted by permission from Ref. [95], Elsevier.

scaffold. In the absence of isocarboxiphos, AP-1 remained hybridized with TWJ-1. Besides, TWJ-2 and TWJ-3 were connected to each other. The open ends of the duplexes caused their adsorption by Fe<sub>3</sub>O<sub>4</sub>@GO, induced no fluorescent signal. This aptasensor with simple operation yet a unique high potential provides a promising strategy for the detection of isocarboxiphos. Also, by combining TWJ structures with the G-quadruplex form of the sequences and constructing a TWJ nanoskeleton with the ends of G-quadruplex, NMM dye can identify G-quadruplex with unique selectivity and emit strong fluorescence. Zhao et al. [88] introduced a fluorescent aptasensor based on the TWJ of DNA strands for detecting acetamiprid. The aptasensor contained four single strands, including AP-1 specific aptamer, SG1 (partially complementary to AP-1), SG2, and SG3. The SG strands were designed so that they could form G-quadruplex structure (SG1/SG3, SG1/SG2, and SG2/SG3) at their ends. In the presence of acetamiprid, AP-1 interacted to it, and the released SG1 formed the TWJ structures with SG2 and SG3, in which the G-quadruplexes were placed in their vicinity. So, NMM dye intercalated to the G-quadruplexes that produced a significant fluorescent response. GO was used to minimize background fluorescence by absorbing free NMM and ssDNA strands in the absence of the target. The aptasensing method is promising for monitoring food and biological resources. In another strategy, Wu et al. [89] designed a one-step biosensor with a competitive mechanism for the rapid and specific in situ detection of cocaine. A new anti-cocaine aptamer called (coc.ap2-GC) was obtained by engineering the nucleic acid sequence of MNS-4.1 aptamer. To strengthen the fluorescence signal, ThT dye was used as a fluorescence marker and competition with cocaine to bind to the aptamer. Converting the pairs of non-contrasting bases in the three stems of the MNS-4.1 aptamer into complementary pairs, and also, adding a pair of the GC sequence to the stem of the aptamer led to the maximum increase in the target affinity. With the binding of cocaine to the DNA TWJ structure of coc. ap2-GC aptamer, the fluorescent response decreased intensely. In the absence of cocaine, intercalating a great number of ThT increased the fluorescence signal. This mix-and-detect aptasensing strategy is cost-effective, rapid, and simple with a high target-binding affinity of the aptamer. The aptasensor can be used as a new facile method with a high potential to detect cocaine within a few seconds.

Antibiotics are small molecules used to inhibit the growth or directly kill bacteria by interfering with bacterial cellular processes such as irreversibly inhibiting protein synthesis [90]. Although antibiotics can be used in practical cases as treatment and prevention goals in medicine and veterinary medicine, but ignoring the standards and uncontrolled use of them, can have destructive effects on human health, such as nephrotoxicity, ototoxicity, and severe allergies [91–94]. For this purpose, our group developed aptasensors based on TWJ nanostructures using two different output signals, fluorescence, and colorimetry, for the sensitive detection of tobramycin. In the first work, we [95] proposed a new fluorescence aptasensor for the measurement of tobramycin based on TWJ nanostructures, which consisted of three engineered strands such that two strands (T1 and T2) were complementary only in the first 15 nucleotides, and the third complementary strand (CS) was hybridized with the ends of T1 and T2 (Fig. 6B). By creating a distance between two strands, the tobramycin binding to its aptamers was improved. PG dye was used as a fluorescent probe with good binding affinity to dsDNA regions. In the absence of tobramycin, a TWJ structure was formed. So, PG could intercalate to three regions (dsDNA), resulting in an intense fluorescent signal. But CS strand could not be hybridized with the free ends of the T1/T2 complex in the presence of tobramycin due to the change of aptamer structure. Hence, PG was only able to intercalate on one region, leading to a great decrease in the fluorescent signal. This

inexpensive, label-free aptasensor can detect tobramycin with high sensitivity within 30 min. In a different investigation, our group [96] engineered a new colorimetric aptasensor based on the TWJ aptamer structure and catalytic properties of AuNPs for the rapid and sensitive detection of tobramycin. Two specific aptamer strands with some additional sequences (T1 and T2) and a complementary strand (CS) were applied to create a TWJ structure. In the absence of tobramycin, the three strands were hybridized that formed a TWJ structure. As a substrate with catalytic activity, AuNPs reduced 4-nitrophenol (4-NP) to 4-aminophenol (4-AP) using sodium borohydride (NaBH<sub>4</sub>), which changed the color of the solution from yellow to colorless. The TWJ structure prevented the access of 4-NP to surfaces of AuNPs and inhibited their catalytic activity through weak interactions. Tobramycin interacted with the S1 and S2 sequences and prevented the formation of TWJ, which resulted in facilitating the activity of AuNPs for reducing 4-NP to 4-AP. It altered the solution color. The TWJ aptasensor with high sensitivity and low detection time can be developed to commercial kits.

Recently, split aptamers in the TWJ form along with signal amplification strategies to improve sensitivity for sensing applications have received considerable attention. In order to solve the challenge of low binding affinity of split aptamers, Chang et al. [97] developed a high throughput colorimetric assay using a signal amplification strategy based on the target-induced recycling assembly of TWJ structures without enzymes to detect estradiol hormone. The sensing system consisted of three DNA strands, split aptamer fragments (SA1 and SA2), and helper DNA (HD), adsorbed on the surface of AuNPs without estradiol. It prevented the aggregation of AuNPs caused by the salt concentrations. SA1 and SA2 strands were hybridized in the presence of estradiol and formed a DNA TWJ-like structure with the help of the HD strand, causing the unstable form of AuNPs and the color change of the solution from red to blue. The label-free nanoplasmonic assay system with high sensitivity, good selectivity, and low-cost has great potential for the in-situ detection of estradiol in complex biological real samples.

Zheng et al. [98] used heterobifunctional aptamers to construct a fluorescent aptasensor for measuring adenosine triphosphate (ATP). The RNA-based aptasensor named Broccoli was developed by the tandem method by combining Broccli-ATPs × 4 and TWJ binding scaffolds (F30 × 3), which led to the expansion of heterofunctional aptamer for improving fluorescence response. The DFHB1 dye was used as a fluorescent reporter and Broccoli's conservative bases were applied as the anchorage sites for the fluorescent reporter. The ATP molecule induced the folding of the aptamer that enabled the linker to form the aptasensor stem. So, the conservative stem of Broccoli was correctly folded, and subsequently, DFHB1 could intercalate to the G-quadruplex region of the Broccoli aptamer that product a fluorescent signal. The genetically encoded aptasensor with biological compatibility functions in a wide range of pH, is a novel method to detect ATP changes with high sensitivity in laboratory conditions.

N<sup>6</sup>-methyladenosine (m6A) epigenetic changes play a vital role in tumor formation and development [99,100]. Yu et al. [101] proposed the use of CRISPR, enzyme-based exponential amplification reaction, and DNAzyme-based TWJ structure for the site-specific detection of M6A RNA. DNAzyme was used for specific cutting of non-methylated RNA, and TWJ/CRISPR system was applied for the high-throughput amplification of the cleavage products. As indicated in Fig. 7, RNA2577-m6A and RNA2577-A as the methylated and non-methylated RNAs, respectively, were exposed to the DNAzyme. The non-methylated adenosine of RNA2577-A was cleaved by DNAzyme, while the methylated site of RNA2577-m6A remained intact. In the presence of RNA2577-m6A, a TWJ structure was formed through hybridization with the template and

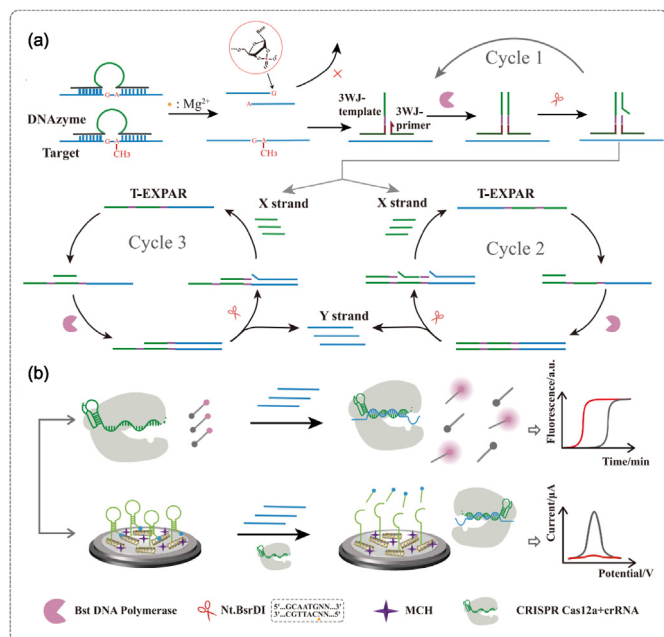


**Fig. 7.** Schematic demonstration of the dual-response aptasensor for detection of M6A RNA. In the presence of RNA2577-m6A, a TWJ structure was formed by interacting with the template and phosphate-modified primer strands. The X strand was produced by the activity of Bst DNA polymerase and Nt.BsrDI endonuclease. A great number of Y strands was obtained as a result of two cyclic amplification processes. The Y strands activated the CRISPR system for cut of two reporter strands, one with the fluorescent dye and quencher molecule at its two ends, and another attached on the electrode surface. Reproduced with permission from Ref. [101], Elsevier.

phosphate-modified primer strands. The 3' end of the TWJ primer was transcribed by Bst DNA polymerase, and then, Nt.BsrDI endonuclease produced a short sequence called X strand. To improve the output signal, the X strand was exposed to T-EXPAR strand that initiated the second amplification cycle. Subsequently, two strands (X and Y) were produced by Nt.BsrDI. Similarly, the X strand initiated another amplification cycle. These successive cycles achieved an exponential amplification mechanism. The produced Y strand was recognized by CRISPR/Cas12a system that activated its *trans*-cleavage behavior for cutting the reporter strand. Subsequently, the fluorescence and electrochemical signals were changed considerably. The proposed method can detect m6A changes down to 1%, which is in biomedical and clinical medicine fields.

#### 4. Aptasensors based on TWJ nanostructure for genes detection

In recent years, aptasensors have become increasingly important for the detection of various targets, such as gene fragments. By combining TWJ aptasensors with signal amplification methods such as loop-mediated isothermal amplification (LAMP), SDA, and DNA-templated metal nanoclusters, the target nucleic acid and gene fragments can be amplified and detected with higher sensitivity and accuracy. LAMP is a nucleic acid amplification technique that amplifies DNA with high specificity and efficiency under isothermal conditions. Guo et al. [102] constructed a portable aptasensor to determine foodborne bacteria genes by coupling the LAMP process, one-step strand exchange (OSD) signal transduction, and TWJ hairpin assembly. First, the LAMP process achieved great copies of the pathogen gene to a detectable concentration. The products with cauliflower-like structures included four types of nucleic acid loops (B, F, Bc, and Fc loops). The F-loop as the

associative trigger activated the formation of the TWJ through a strand replacement reaction. It possessed two domains of  $\alpha$  and  $\beta$ , in which the latest domain was hybridized with the transducer probe (TP). So, it provided a suitable distance for the  $\alpha$  domain from domain 2-3 in the TP to proceed the downstream formation of the TWJ assembly. By adding the H1 and H2 strands and proceeding consecutive OSD processes, the H1/H2 hybrid was formed as the product. The trigger strand also was released for opening another H1 stand as a catalyst. Besides, the embedded domain 2 in the H1 stem was released for involving in linear stage together with domain 5-6. Another OSD process was started by the domain 2-5-6 that replaced the inverse-modified oligonucleotide (TmINVeF) attached on magnetic beads. After magnetic separation, the TmINVeF was released into the supernatant that triggered the catalytic process of the sucrose transduction to glucose. By recording the glucose concentration by using a hand-held glucose meter, the *ompA* targeting gene could be determined sensitively.

SDA is a powerful nucleic acid amplification technique that can amplify target DNA (ssDNA or dsDNA), under isothermal conditions without the need for thermal cycling [103]. Therefore, the amplified target DNA can be quantified through various strategies such as fluorescence method with rapid detection and high sensitivity [104–106]. Liu et al. [107] designed an ultrasensitive biosensor to identify the CaMV 35S promoter based on proximity extension mediated multiple cascade strand displacement amplification accompanied with CRISPR/Cpf1 (PE-MC/SDA-CRISPR/Cpf1). As shown in Fig. 8A, the biosensor included two primers (P1 and P2) with two additional T bases on the P2 primer for forming a TWJ connection only in the presence of the target with the help of Klenow fragment (KF) polymerization. The process increased the thermodynamic stability and decreased the background signal. The P1 strand possessed a restriction site that was cut by Nt. BbvCI endonuclease. It activated the repetition of the amplification cycle that produced a great number of a short sequence called M strand. The M strand was hybridized with the SDA strand (ST). Then, the second amplification process was initiated with the function of KF polymerase and Nt. BbvCI, which obtained two new strands called X and Y. The X strand was included in another amplification cycle. The Y strand activated the CRISPR/Cpf1 system for cleavage of the FQ reporter strand that recovered the fluorescent signal. This strategy can identify a wider range of nucleic acids by reprogramming.

Tian et al. [108] proposed a universal platform for nucleic acid detection based on a two-step amplification mechanism based on the transcription of crRNA and *trans*-cleavage activity of Cas12a (Fig. 8B). The platform comprised two ssDNA proximity probes including the template probe and extension probe (shorter than the template probe). The template probe consisted of four parts, including a region for binding to the target, a short complementary sequence for the extension probe, a T7 RNA polymerase promoter, and a transcription template of crRNA. When the ssDNA target was present, it was bound to the template and extension probes that created a DNA TWJ structure. Subsequently, the expansion probe was transcribed by the KF enzyme. A double-stranded T7RNA polymerase promoter sequence was activated that produced multiple crRNAs. The crRNA, dsDNA activator containing PAM sequence, and Cas12a formed a ternary complex that activated Cas12a for digestion of the FAM reporter. As a result, the fluorescent dye in the reporter was separated from the BHQ-1 quencher, obtaining a fluorescent signal. This ultra-sensitive platform with the detection limit of 417 fM, cost-effectiveness, and simplicity can be used to identify a wide range of DNAs and RNAs in future investigations.

DNA-templated metal nanoclusters are fluorescent nanomaterials synthesized by binding metal ions to DNA templates. Shen et al. [109] designed a new strategy for target DNA detection

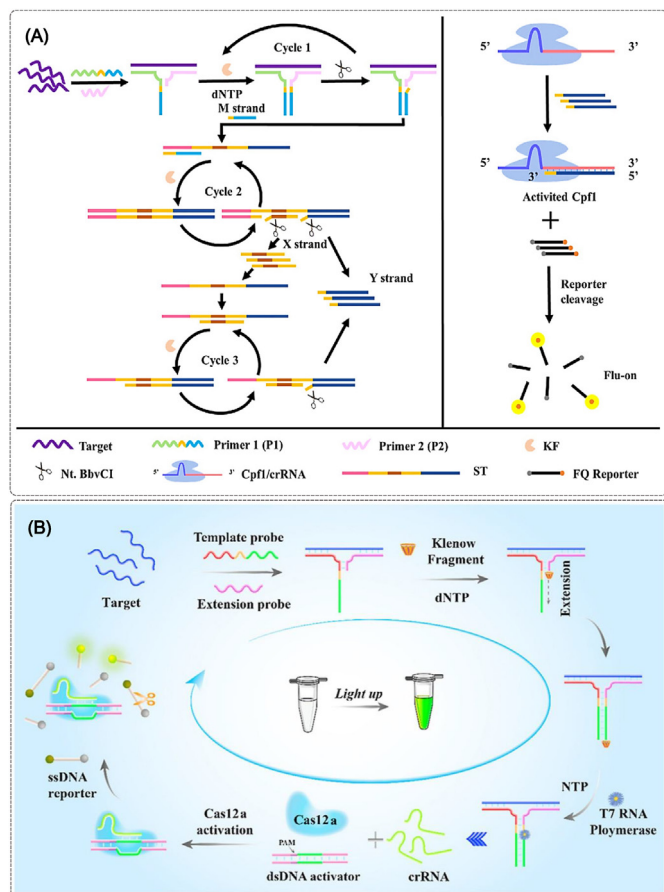


**Fig. 8.** (A) The principal representation of the fluorescent biosensor for the CaMV 35S detection based on cascade strand displacement amplification process accompanied with CRISPR/Cpf1. Reproduced with permission from Ref. [107], Elsevier. (B) The schematic illustration of the CRISPR/Cas12a nucleic acid sensing platform based on the crRNA transcription assisted by the TWJ structure. By adding the DNA target, it interacted with the probes and formed a TWJ structure. Afterward, T7RNA polymerase produced multiple crRNAs, which formed a ternary complex accompanied by dsDNA activator and Cas12a. Consequently, the FAM reporter was digested which recovered the fluorescent signal. Represented by permission from Ref. [108], Elsevier.

based on recycling amplification promoted by TWJ. In this case, the DNA hairpin was used as a template for forming silver nanoclusters (AgNCs) by adding  $\text{Ag}^+$  and  $\text{NaBH}_4$ , which produced a strong fluorescence signal. The DNA hairpin possessed a single string (13 nucleotides) at the 3'-end containing the target DNA recognition motif, which acted as a molecular beacon (MB) foundation for the formation of the TWJ. In the presence of the target DNA, it was connected to the hairpin probe and formed a TWJ structure. Then, it was decomposed and digested by exonuclease (Exo-III) from the 5' side. As a result, there was no probe to make AgNCs, which produced a very weak signal. The clever use of a TWJ structure increased the digestion efficiency of Exo-III by 9 times at 37 °C. This low-cost and label-free method with a high quantum efficiency (69.2%) can be used to identify DNA types by manipulating the recognition motif of the probe.

## 5. Aptasensors based on TWJ nanostructure for cells detection

Microbial pathogens are responsible for a wide range of infectious diseases, including respiratory infections, gastroenteritis, and liver infections [110–112]. The ability to detect these pathogens

quickly and accurately is critical for disease management and control. TWJ-based aptasensors have been developed for the detection of several viral and bacterial pathogens, including severe acute respiratory syndrome coronavirus 2 (SARS-CoV-2), *Salmonella Typhi* (*S. Typhi*), *Escherichia coli* (*E. coli*), and *Mycobacterium tuberculosis* complex (MTC) [113–115]. For this purpose, Yu et al. [116] fabricated a novel electrochemical biosensor for monitoring hepatitis virus B (HBV) based on the LAMP for TWJ transduction. The rtN236T mutation as a miss-encoded transcriptase segment of HBV DNA asparagine replaced by threonine was selected as a model gene target, because its existence fails adefovir dipivoxil therapy. Fig. 9 indicates the sensing mechanism of the developed biosensor. The rtN236T mutant was achieved from the loop-mediated LAMP amplicons that could form a TWJ structure by involving the S1 and S2 strands. This resulted in the release of the S3 toehold region that triggered the Exo-III assisted catalyzed hairpin assembly (CHA) with the cooperation of H1 strand and methylene blue (MB)-modified H2 probe (MB-H2). Consequently, a great number of the MB-P short strands and released H1 were obtained as a result of the degradation of MB-H2 sequence. The released H1 continued the CHA cycle. The MB-P strands were hybridized with the hairpin-structured SH-P strands on the electrode surface, which strengthened the electrochemical response through decreasing the distance between the electrode and MB molecules.

Early detection of SARS-CoV-2 in infected people has become a global challenge to control the epidemic of this disease [117–119]. Han et al. [120] designed a TWJ-induced exponential rolling circle amplification (eRCA) platform with matrix-assisted laser desorption/ionization time-of-flight mass spectrometry (MALDI-TOF MS) hybrid detection. This highly sensitive platform based on TWJ nanoskeleton can detect SARS-CoV-2 pseudovirus at 55 °C within 30 min in the different media. The TWJ structure included a DNA template with a complementary sequence called RC-primer. In the presence of SARS virus RNA, it was attached to the primer and template strands that formed a stable TWJ structure with a key role in the production of the enrichment products for MALDI-TOF MS. During the amplification cycle, numerous RC-primers were produced by Vent (exo-) DNA polymerase and Nt.BspQI nicking endonuclease. The produced primers were hybridized with the RC-template, and a linear eRCA cascade process was initiated by the activity of the polymerase. So, a long sequence of the RC-template

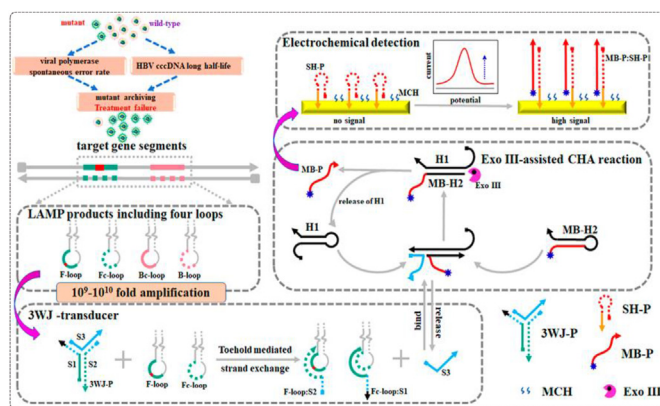


**Fig. 9.** Schematic interpretation of the electrochemical biosensor for detecting rtN236T mutant. After obtaining a great number of the target through the loop-mediated LAMP process, it formed the TWJ structure by interacting with the S1 and S2 strands. So, the toehold segment of the S3 strand was released that initiated the CHA accompanying with the H1 and MB-H2 sequences. The MB-H2 strands were cleaved to short ones that could be hybridized by the SH-P strands on the electrode surface. Consequently, the electrochemical signal increased significantly. Represented by permission from Ref. [116], American Chemical Society.

was produced, and subsequently, was cut by Nt. BstNBI and Nt.BspQI endonucleases. Consequently, numerous short ssDNA was formed, which acted as the triggers for the initiation of the subsequent eRCA loops. In this way, a large number of products were obtained for MALDI-TOF MS detection of SARS-CoV-2 with high sensitivity.

The Middle East Respiratory Syndrome Coronavirus (MERS-CoV), a strain of the coronavirus that causes Middle East Respiratory Syndrome (MERS), was first reported in Saudi Arabia in 2012 (Isolation of a Novel Coronavirus from a Man with Pneumonia in Saudi Arabia) [121,122]. To prevent the spread of MERS-CoV, Kim et al. [123] designed a sensitive detection method to identify MERS-CoV with a dual detection method based on SERS and electrochemistry techniques. As shown in Fig. 10A, in the sensing system, the MERS nanovesicle (MERS-NV) was analyzed instead of MERS-CoV, which has the spike protein (S) of MERS-CoV and does not contain genetic material. The multifunctional DNA TWJ aptamer with three independent functional groups (MERS aptamer, methylene blue, and thiol group) and graphene oxide-molybdenum disulfide (GO-MoS<sub>2</sub>) nanocomposite was utilized for the fast electron transfer and SERS signal enhancement, which could detect MERS-NV in phosphate buffer (PBS) and saliva. The sensing method showed the high potential of TWJ aptamers in diagnostic systems

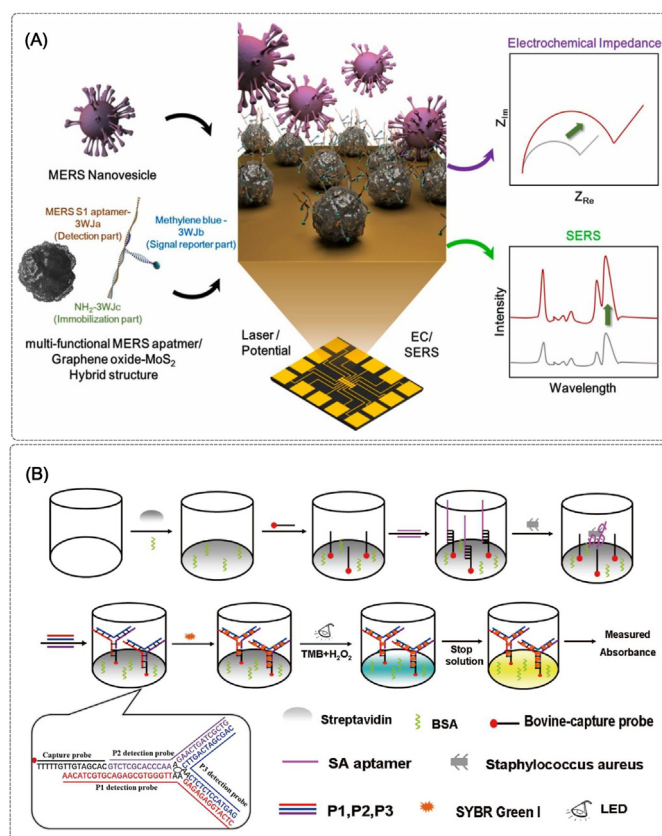


**Fig. 10.** (A) Action mechanism of MERS-NVs assay system on an Au substrate. In the aptasensing system, the specific aptamer of the spike protein for MERS-NVs was obtained by SELEX and stabilized with three functional groups by thiol group on GO-MoS<sub>2</sub> hybrid nanocomposite, and the modified electrode was developed based on Au micro-gap. Reproduced with permission from Ref. [123], Elsevier. (B) Schematic depiction of the developed assay for monitoring *S. aureus*. In the presence of *S. aureus*, the TWJ nanostructure was hybridized with the single-strand capture probe from the complementary region on the P1 strand. By assembling a substrate suitable for SG I, the dsDNA-SG I complex was created, which catalyzed the oxidation of tetramethylbenzidine (TMB), leading to a yellow color change in the solution. Reproduced with permission from Ref. [124], Springer Nature.

by having three different and independent functional groups for substrate connection, target detection, and signal reporter in a single structure.

Considering the wide range of TWJ nanostructures in sensing systems, Yu et al. [124] designed a colorimetric platform for the rapid diagnostic of *Staphylococcus aureus* (*S. aureus*) with high sensitivity (Fig. 10B). In this aptamer-based assay, the DNA TWJ nanostructure was used for signal amplification and SYBR Green I (SG I) for photocatalytic activity, which has a high throughput in the simultaneous detection of 96 samples, and also, is a highly sensitive, fast, and nanoparticle-free method. The biosensor with direct detection of *S. aureus* bacteria in 5.5 h and great linear range, and a low detection limit, has excellent potential in screening pathogenic microorganisms for clinical applications and food control. In addition to DNA aptamers, the RNA types are also efficient for developing TWJ-based aptasensors, as Moon et al. [125] designed various RNA TWJ structures for the detection of S-adenosylmethionine in mammalian real samples.

TWJ-based aptasensors can also be used to detect cancer cells by integrating TWJ scaffolds as a final product in CHA cycles. This method is a type of nucleic acid amplification technique that can enhance the sensitivity and specificity of biosensors [126,127]. Ravan et al. [128] engineered a TWJ-based hairpin DNA cascade amplifier (HDCA) biosensor for the detection of human leukemic lymphoblast cells (CCRF-CEM) with high sensitivity and selectivity. The designed strategy based on enzyme-free signal amplification and aggregation of AuNPs is 4 times higher sensitive than the approaches based on enzyme-mediated signal amplification. Protein tyrosine kinase 7 (PTK7) is overexpressed in T-cell acute lymphocytic leukemia (T-ALL). This protein acts as a useful biomarker to detect blood cancer cells. The aptasensor system for detecting PTK7 included three hairpin DNA monomers modified by biotin at 3' ends and a chimeric aptamer with a recognition domain of PTK7 and streptavidin-modified AuNPs (Au-SA) as a signal transducer. By its binding to PTK7, the chimeric aptamer acted as an initiator for the CHA process between the three hairpin monomers to make the TWJ structures. Au-SA formed a cross-linking network in the presence of the TWJ structures through the non-covalent interactions between biotin-streptavidin, which led to the aggregation of AuNPs and induced red-shifting. Compared to the other methods such as fluorescence or electrochemical, the HDCA method based on colorimetry provides lower cost, convenient, and fast diagnosis without the need for special equipment.

The summary of the scientific reports about the categories of the TWJ-based biosensing assays is given in Table 1. Table 1 highlights the ultrasensitivity of the TWJ-based aptasensors for detecting various targets (e.g., disease biomarkers, drugs, toxins, and so on) even at attomolar levels. Table 1 clarifies that TWJ-assisted aptasensors are beneficial for multiple target detection by using different signal reporters and probe pieces. Based on Table 1, most of the TWJ-included aptasensors are based on fluorescent and electrochemical output signals. So, developing colorimetric approaches with the cooperation of TWJ nanostructures is novel for naked-eye monitoring of target analytes.

## 6. In-depth discourse and conclusion

With their extraordinary potency in diagnosis, healthcare monitoring, food safety, and environmental proceedings, biosensing assays are a peculiar research focus in scientific society. Also, designing non-invasive, simple, and easy-to-apply biosensing tools based on TWJ nanostructures is promising. Our detailed study highlights the advance in the aptasensing strategies based on TWJ assemblies. According to our study, TWJ-based aptasensors possess a wide range of diagnostic functions that can detect different types

**Table 1**  
Summary of TWJ-based aptasensors extracted from the literature to detect and control a wide range of targets.

No.	Category	Method	Target	Detection Limit	Detection Range	Real Sample	Reference
1	Biomarker	Electrochemical	miRNA-21	3.6 fM	10 fM-10 nM	Lysates extracted from MCF-7 and HeLa cells	[57]
2	Biomarker	Electrochemical	miRNA-21	0.077 fM	0.1 fM-100 pM	Human plasma	[58]
3	Biomarker	Electrochemiluminescence	miRNA-21	96 aM	100 aM-1 nM	Human plasma	[59]
4	Biomarker	Electrochemical	miRNA-182-5p	31.13 aM	0.1 fM-1 nM	Human serum	[60]
5	Biomarker	Electrochemical	Exosomal miRNA	7.3 aM	10 aM-0.1 pM	Human serum	[61]
6	Biomarker	Fluorescence	miR-21, miR-27a and miR-375	0.116 µg/mL, 0.125 µg/mL and 0.287 µg/mL	5–140 nM, 2–100 nM and 7–70 nM	Human serum	[65]
7	Biomarker	Fluorescence	Let-7a	68 pM	0.2–20 nM	Human serum	[71]
8	Biomarker	Fluorescence	miRNA-153	1 fM	1 fM-1 µM	Human blood	[72]
9	Biomarker	EC-SERS	miRNA-155	0.06 fM	0.1 fM-1 nM	Human serum	[73]
10	Biomarker	Fluorescence	miRNA-21 and miRNA-141	Not Reported	10 pM-10 nM	Blood	[77]
11	Biomarker	Electrochemical	ctDNA	48 aM	100 aM-1 nM	Serum and cell	[85]
12	Biomarker	SERS	CRP	2.23 pM in phosphate-buffered saline, and 3.11 pM in human serum	100 nM to 1 pM	Human serum	[86]
13	Small molecule	Fluorescence	Isocarbophos	3.38 nM	10–500 nM	Apple and lake water	[87]
14	Small molecule	Fluorescence	Acetamiprid	5.73 nM	0–500 nM	Apple and lake water	[88]
15	Small molecule	Fluorescence	Cocaine	250 nM	1–500 µM	Human urine and saliva	[89]
16	Small molecule	Fluorescence	Tobramycin	21.86 nM	80 nM-2 µM	Human serum	[95]
17	Small molecule	Colorimetric	Tobramycin	1.16 µM	4–32 µM	Milk and human serum	[96]
18	Small molecule	Colorimetric	Estradiol	0.7 nM	0.7–2000 nM	Urine	[97]
19	Small molecule	Fluorescence	ATP	0.44 nM	10–250 nM	Mammalian cells	[98]
20	Small molecule	Fluorescence	M6A RNA	1%	1%–40% fraction	Human serum	[101]
21	Gene	Electrochemical	OmpA gene	20 copies (aM concentration)	20–2000 copies	Not reported	[102]
22	Gene	Fluorescence	CaMV 35S promotor	14.4 fM	50 fM-10 pM and 10 pM–500 pM	Plant genome	[107]
23	Gene	Fluorescence	Nucleic acid	417 fM	500 fM-100 pM	Human body	[108]
24	Gene	Fluorescence	DNA hairpin	2.8 nM	5–50 nM	Not reported	[109]
25	Cell	Electrochemical	Hepatitis B virus	Down to 2 copies/µL	2–20000 copies/µL	Human serum	[116]
26	Cell	Laser desorption/ionization time-of-flight mass spectrometry	SARS CoV-2	1 pM	1 pM-0.1 µM	Water, saliva, and urine	[120]
27	Cell	SERS/EC	MERS-nanovesicle	0.525 pg/mL (SERS) and 0.645 pg/mL (EIS)	1 pg/mL-100 ng/mL	Artificial saliva	[123]
28	Cell	Colorimetric	<i>Staphylococcus aureus</i>	81 CFU/mL	10 <sup>2</sup> –10 <sup>7</sup> CFU/mL	Milk	[124]
29	Cell	Colorimetric	Human leukemic lymphoblast cell	10 cells	25-10 <sup>7</sup> cells	Not reported	[128]

of targets, including genes, disease biomarkers, cancer cells, microbial pathogens, small molecules, metal ions, and so on. Relying on the accumulation of negative charge in the center of the TWJ structures due to phosphate groups, aptasensors based on TWJ assemblies are promising for the detection of cationic species. Besides, TWJ-based aptasensors can be intelligently designed with three independent arms, each associated with different signal output modes such as colorimetric, fluorescence, electrochemical, and SERS, to enable simultaneous identification of multiple targets, making them highly effective multifunctional sensing tools. Although TWJ nanostructures exhibit desirable properties, their formation poses certain challenges. Due to the accumulation of negative charges at the center of the three arms of TWJ, selecting an appropriate buffer to neutralize these charges and create a stable structure is crucial. Additionally, preparing sequences with specific temperature cycles to generate hybrids in complementary regions, optimizing long incubation times, and storing at low temperatures are other challenging aspects in the construction and maintenance of TWJ structures. Aptasensing strategies based on TWJ nanostructures can detect ultralow levels of targets even at attomolar or

femtomolar levels, as well as was applied by Bian et al. [55] to detect PML/RAR $\alpha$  fusion gene at the femtomolar concentration levels. Paper-based microfluidic aptasensors, which benefit easy-to-carry biocompatible materials as sensing substrate, are efficient for low-cost, fast, real-time, on-site, and portable target detection. Hence, combining paper-based microfluidic biosensing arrays with the advantageous TWJ nanostructures presents novel diagnostic devices, promising for development in the near future. Bacterial cellulose nanofibers are promising bio-platforms for the construction of portable biosensing devices based on their advantages of renewability, biodegradability, biocompatibility, high mechanical strength, and ultrafine matrix for easy carrying. Hence, incorporating TWJ nanostructures with cellulose nanofiber skeletons is a future prospect to develop easy-to-carry sensing platforms for on-site target detection. To now, some amplification mechanisms have been applied to construct colorimetric TWJ-based biosensing approaches. For example, the CHA mechanism as a method for producing hairpin DNA cascade amplifiers can act as an inhibitor against the salt-induced aggregation of AuNPs. Besides, the CHA technique can be combined with sol-gel assays for

encapsulating AuNPs as a tracer agent of the target. Also, the RCA strategy is an isothermal amplification approach to generate long single-stranded DNA or RNA products with repeated sequences, which can achieve ultra-sensitive, and robust biosensing assays in combination with TWJ nanostructures. TWJ DNA skeletons can control the enzyme-like activity of AuNPs, which is superb for developing colorimetric biosensing assays. They also can mediate G-quadruplex-hemin DNAzyme for inducing oxidation catalytic activity [129]. The TWJ-mediated biosensors are inimitable with representing supreme sensitivity, facile usage, non-toxicity, reliability, cost-effectiveness, and uncomplicated apparatus. As a future idea, TWJ DNA pockets can join liquid crystals (LCs) as an external stimuli-supersensitive signal indicator to offer portable biosensing devices for naked-eye target monitoring. Although various LC-included biosensors have been represented for monitoring different targets [130], no TWJ nanostructure is along with LC-based aptasensors, making it promising for the future design of LC-based biosensing tools mediated by TWJ structures. To have fluorescent detection of targets, different fluorophore molecules can be pinned into DNA branches of TWJ-based biosensors; however, labeling process increases the cost of dye-labeled TWJ sensing platforms. Hence, intercalating dye molecules can reduce production costs. Moreover, by programming T-rich or C-rich arms of TWJ skeletons can attain templates for anchoring multicolor CuNPs or AgNPs that are smart label-free multicolor fluorescent TWJ assays. Applying diverse nanomaterials in the form of nanocage, nanoflower, core-shell, metallic frameworks, carbonic networks, dots, and nanosheets is promising to achieve novel boosted fluorescent TWJ aptasensors as well as electrochemical ones. Based on the advantages of 2D nanomaterials, MoS<sub>2</sub> sheets are efficient skeletons for developing TWJ-based aptasensor. Accordingly, cooperation of other transition metal dichalcogenide nanostructures (e.g., WS<sub>2</sub>, WSe<sub>2</sub>, MoSe<sub>2</sub>, and so on) with TWJ DNAs attains smart architecting of nano-biosensing gadgets. Hopefully, TWJ aptamer buildings with the superb stability and conformational versatility can be coupled with autonomous wearable sensing strategies for universal target analysis, as a future prospect.

### Declaration of competing interest

The authors declare that they have no known competing financial interests or personal relationships that could have appeared to influence the work reported in this paper.

### Data availability

The authors are unable or have chosen not to specify which data has been used.

### Acknowledgment

The authors gratefully acknowledge the financial support provided by Mashhad University of Medical Sciences and Ferdowsi University of Mashhad for this study. This research was extracted from the Master's thesis of Mr. Hamed Zahraee. We would also like to express our gratitude to Mr. Morteza Alinezhad Nameghi for his valuable assistance in designing the graphical abstract.

### References

- [1] A.D. Ellington, J.W. Szostak, *Nature* 346 (1990) 818.
- [2] C. Tuerk, L. Gold, *Science* 249 (1990) 505.
- [3] J. Zhou, J. Rossi, *Nat. Rev. Drug Discov.* 16 (2017) 181.
- [4] T. Sakamoto, E. Ennifar, Y. Nakamura, *Biochimie* 145 (2018) 91.
- [5] T.T.-Q. Nguyen, E.R. Kim, M.B. Gu, *Biosens. Bioelectron.* 198 (2022), 113835.
- [6] K.-H. Leung, B. He, C. Yang, C.-H. Leung, H.-M.D. Wang, D.-L. Ma, *ACS Appl.*

- Mater. Interfaces* 7 (2015), 24046.
- [7] M. Fadeev, M.P. O'Hagan, Y. Biniuri, I. Willner, *J. Phys. Chem. B* 126 (2022) 8931.
- [8] S. Centane, T. Nyokong, *J. Inorg. Biochem.* 230 (2022), 111764.
- [9] A. Chen, S. Yang, *Biosens. Bioelectron.* 71 (2015) 230.
- [10] A.D. Keefe, S. Pai, A. Ellington, *Nat. Rev. Drug Discov.* 9 (2010) 537.
- [11] L. Li, S. Xu, H. Yan, X. Li, H.S. Yazd, X. Li, T. Huang, C. Cui, J. Jiang, W. Tan, *Angew. Chem. Int. Ed.* 60 (2021) 2221.
- [12] V. Thiviyanathan, D.G. Gorenstein, *Proteomics Clin. Appl.* 6 (2012) 563.
- [13] H. Zahraee, A. Mehrzad, K. Abnous, C.-H. Chen, Z. Khoshbin, A. Verdian, *Recent Advances in Aptasensing Strategies for Monitoring Phycotoxins: Promising for Food Safety*, 2023.
- [14] A. Schwenger, H. Griesser, C. Richert, *DNA-based Nanostructuring with Branched Oligonucleotide Hybrids*, 2014, p. 375.
- [15] F. Zhang, J. Nangreave, Y. Liu, H. Yan, *J. Am. Chem. Soc.* 136 (2014), 11198.
- [16] H. Zahraee, Z. Khoshbin, M. Ramezani, M. Alibolandi, K. Abnous, S.M. Taghdisi, *Spectrochim. Acta Mol. Biomol. Spectrosc.* 290 (2023), 122305.
- [17] W.C. Tse, D.L. Boger, *Chem. Biol.* 11 (2004) 1607.
- [18] X. Chen, L. Zhang, X. Shao, W. Gong, T. Shi, J. Dong, Y. Shi, S. Shen, Y. He, J. Qin, J. Lu, Q. Jiang, B. Guo, *Adv. Funct. Mater.* 32 (2022), 2109460.
- [19] Y.-A. Shieh, S.-J. Yang, M.-F. Wei, M.-J. Shieh, *ACS Nano* 4 (2010) 1433.
- [20] Q. Mou, X. Xue, Y. Ma, M. Banik, V. Garcia, W. Guo, J. Wang, T. Song, L.-Q. Chen, Y. Lu, *Sci. Adv.* 8 (2022), eabo0902.
- [21] Z. Khoshbin, H. Zahraee, J. Zamanian, A. Verdian, M. Ramezani, M. Alibolandi, K. Abnous, S.M. Taghdisi, *Anal. Chim. Acta* 1236 (2022), 340588.
- [22] Y. Liu, L. Kong, H. Li, R. Yuan, Y. Chai, *Anal. Chem.* 94 (2022) 6819.
- [23] N.C. Seeman, *J. Theor. Biol.* 99 (1982) 237.
- [24] N.C. Seeman, *Annu. Rev. Biochem.* 79 (2010) 65.
- [25] I.T. Seemann, V. Singh, M. Azarkh, M. Drescher, J.S. Hartig, *J. Am. Chem. Soc.* 133 (2011) 4706.
- [26] N.M. Danesh, R. Yazdian-Robati, M. Ramezani, M. Alibolandi, K. Abnous, S.M. Taghdisi, *Sensor. Actuator. B Chem.* 256 (2018) 408.
- [27] Y. Takezawa, M. Shionoya, *Front. Chem.* 7 (2020).
- [28] N.C. Seeman, *Structural DNA Nanotechnology*, Cambridge University Press, Cambridge, 2016.
- [29] Y. Xu, X. Bian, Y. Sang, Y. Li, D. Li, W. Cheng, Y. Yin, H. Ju, S. Ding, *Sci. Rep.* 6 (2016), 32370.
- [30] E. Hosseinzadeh, H. Ravan, A. Mohammadi, R. Mohammad-rezaei, A. Norouzi, H. Hosseinzadeh, *Biosens. Bioelectron.* 117 (2018) 567.
- [31] Y. Dong, C. Yao, Y. Zhu, L. Yang, D. Luo, D. Yang, *Chem. Rev.* 120 (2020) 9420.
- [32] Y. Li, Y.D. Tseng, S.Y. Kwon, L. d'Espaux, J.S. Bunch, P.L. McEuen, D. Luo, *Nat. Mater.* 3 (2004) 38.
- [33] R.M. Young, A.P.N. Singh, A.K. Thazhathveetil, V.Y. Cho, Y. Zhang, N. Renaud, F.C. Grozema, D.N. Beratan, M.A. Ratner, G.C. Schatz, Y.A. Berlin, F.D. Lewis, M.R. Wasielewski, *J. Am. Chem. Soc.* 137 (2015) 5113.
- [34] J.-Y. He, H.-L. Deng, X. Shang, C.-L. Yang, S.-Y. Zuo, R. Yuan, H.-Y. Liu, W.-J. Xu, *Anal. Chem.* 94 (2022) 8041.
- [35] Y. Zhou, Y. Zeng, D. Zhang, P. Qi, Y. Wang, Y. Xin, Y. Sun, *Sensor. Actuator. B Chem.* 374 (2023), 132749.
- [36] O. Alkhamis, W. Yang, R. Farhana, H. Yu, Y. Xiao, *Nucleic Acids Res.* 48 (2020), e120.
- [37] J.E. Ladbury, J.M. Sturtevant, N.B. Leontis, *Biochemistry* 33 (1994) 6828.
- [38] M.P. Leveille, T. Tran, G. Dingillo, B. Cannon, *Biophys. Chem.* 245 (2019) 25.
- [39] B.M. Laing, R.L. Juliano, *ChemBiochem* 16 (2015) 1284.
- [40] S. Muhuri, K. Mimura, D. Miyoshi, N. Sugimoto, *J. Am. Chem. Soc.* 131 (2009) 9268.
- [41] C. Yang, H. Deng, J. He, X. Zhang, J. Gao, X. Shang, S. Zuo, R. Yuan, W. Xu, *Biosens. Bioelectron.* 199 (2022), 113871.
- [42] F. Zhang, S. Jiang, S. Wu, Y. Li, C. Mao, Y. Liu, H. Yan, *Nat. Nanotechnol.* 10 (2015) 779.
- [43] C.-M. Chien, P.-C. Wu, R. Satange, C.-C. Chang, Z.-L. Lai, L.D. Hagler, S.C. Zimmerman, M.-H. Hou, *J. Am. Chem. Soc.* 142 (2020), 11165.
- [44] Y. Li, J. Pei, X. Lu, Y. Jiao, F. Liu, X. Wu, J. Liu, B. Ding, *J. Am. Chem. Soc.* 143 (2021), 19893.
- [45] Y. Yao, N. Li, X. Zhang, J. Ong'achwa Machuki, D. Yang, Y. Yu, J. Li, D. Tang, J. Tian, F. Gao, *ACS Appl. Mater. Interfaces* 11 (2019), 13991.
- [46] A.J. Van Riesen, J. Le, S. Slavkovic, Z.R. Churcher, A.A. Shoara, P.E. Johnson, R.A. Manderville, *ACS Appl. Bio Mater.* 4 (2021) 6732.
- [47] H.-H. Pang, C.-Y. Huang, P.-Y. Chen, N.-S. Li, Y.-P. Hsu, J.-K. Wu, H.-F. Fan, K.-C. Wei, H.-W. Yang, *ACS Nano* 17 (2023) 10407.
- [48] J. Han, Y. Cui, Z. Gu, D. Yang, *Biomaterials* 273 (2021), 120846.
- [49] J. Zhu, L. Zhang, Z. Zhou, S. Dong, E. Wang, *Anal. Chem.* 86 (2014) 312.
- [50] M. Mohammadniaei, J. Yoon, H.K. Choi, V. Placide, B.G. Bharate, T. Lee, J.-W. Choi, *ACS Appl. Mater. Interfaces* 11 (2019) 8779.
- [51] A. Krissanaprasit, C.M. Key, S. Pontula, T.H. LaBeau, *Chem. Rev.* 121 (2021), 13797.
- [52] H. Chai, Y. Tang, P. Miao, *Anal. Chem.* 94 (2022) 9975.
- [53] L. Zhang, S. Guo, J. Zhu, Z. Zhou, T. Li, J. Li, S. Dong, E. Wang, *Anal. Chem.* 87 (2015), 11295.
- [54] F. Ma, Y. Chen, Y. Zhu, J. Liu, *Talanta* 194 (2019) 114.
- [55] X. Bian, B. Guo, M. Zhao, D. Han, W. Cheng, F. Song, S. Ding, *ACS Appl. Mater. Interfaces* 11 (2019) 3715.
- [56] W. Wu, X. Yu, J. Wu, T. Wu, Y. Fan, W. Chen, M. Zhao, H. Wu, X. Li, S. Ding, *Biosens. Bioelectron.* 175 (2021), 112835.
- [57] L. Jiang, Y. Yang, Y. Lin, Z. Chen, C. Xing, C. Lu, H. Yang, S. Zhang, *Analyst* 145

- (2020) 3353.
- [58] Z. Hu, B. Zhao, P. Miao, X. Hou, F. Xing, Y. Chen, L. Feng, *J. Electroanal. Chem.* 880 (2021), 114861.
- [59] X. Hou, Z. Suo, Z. Hu, X. Zhang, Y. Chen, L. Feng, *J. Electroanal. Chem.* 880 (2021), 114935.
- [60] Y. Chang, S. Xu, Y. Li, W. Hu, H. Li, R. Yuan, Y. Chai, *Anal. Chem.* 93 (2021), 12981.
- [61] P. Miao, Y. Tang, *Anal. Chem.* 92 (2020), 12026.
- [62] D. Bautista-Sánchez, C. Arriaga-Canon, A. Pedroza-Torres, I.A. De La Rosa-Velázquez, R. González-Barrios, L. Contreras-Espinosa, R. Montiel-Manríquez, C. Castro-Hernández, V. Fragos-Ontiveros, R.M. Álvarez-Gómez, L.A. Herrera, *Mol. Ther. Nucleic Acids* 20 (2020) 409.
- [63] W. Tang, J. Zhu, S. Su, W. Wu, Q. Liu, F. Su, F. Yu, *PLoS One* 7 (2012), e51702.
- [64] F. Zehentmayr, C. Hauser-Kronberger, B. Zellinger, F. Hlubek, C. Schuster, U. Bodenhofer, G. Fastner, H. Deutschmann, P. Steiningner, R. Reitsamer, T. Fischer, F. Sedlmayer, *Clin. Epigenet.* 8 (2016) 28.
- [65] H. Wang, D. He, K. Wan, X. Sheng, H. Cheng, J. Huang, X. Zhou, X. He, K. Wang, *Analyst* 145 (2020) 3289.
- [66] C.D. Johnson, A. Esquela-Kerschner, G. Stefani, M. Byrom, K. Kelnar, D. Ovcharenko, M. Wilson, X. Wang, J. Shelton, J. Shingara, L. Chin, D. Brown, F.J. Slack, *Cancer Res.* 67 (2007) 7713.
- [67] K.J. Cho, J. Song, Y. Oh, J.E. Lee, *Mol. Cell. Neurosci.* 68 (2015) 167.
- [68] B. Brueckner, C. Stresemann, R. Kuner, C. Mund, T. Musch, M. Meister, H. Stültmann, F. Lyko, *Cancer Res.* 67 (2007) 1419.
- [69] K. Liu, C. Zhang, T. Li, Y. Ding, T. Tu, F. Zhou, W. Qi, H. Chen, X. Sun, *Int. J. Oncol.* 46 (2015) 2526.
- [70] X.-B. Long, G.-B. Sun, S. Hu, G.-T. Liang, N. Wang, X.-H. Zhang, P.-P. Cao, H.-T. Zhen, Y.-H. Cui, Z. Liu, *Oncol. Rep.* 22 (2009) 1189.
- [71] L. Zhang, X. Liu, X. Xu, N. Zhang, W. Jiang, *Sensor. Actuator. B Chem.* 327 (2021), 128942.
- [72] J. Cui, H. Han, J. Piao, H. Shi, D. Zhou, X. Gong, J. Chang, *ACS Appl. Mater. Interfaces* 12 (2020), 34130.
- [73] T. Lee, M. Mohammadniaei, H. Zhang, J. Yoon, H.K. Choi, S. Guo, P. Guo, J.-W. Choi, *Adv. Sci.* 7 (2020), 1902477.
- [74] H. Gao, K. Zhang, X. Teng, J. Li, *TrAC, Trends Anal. Chem.* 121 (2019), 115700.
- [75] L. Xu, J. Duan, J. Chen, S. Ding, W. Cheng, *Anal. Chim. Acta* 1148 (2021), 238187.
- [76] N. Luo, Q. Xia, L. Zhang, Y. Zhang, L. Huang, Y. Zhang, J. Zhao, S. Ding, W. Cheng, *Anal. Chim. Acta* 1067 (2019) 129.
- [77] C.-y. Qu, L.-s. Zhou, L.-h. Shu, Q. Huang, *ACS Omega* 6 (2021) 3330.
- [78] M.J. Duffy, J. Crown, *Clinical Chemistry* 68 (2022) 1381.
- [79] F. Yang, J. Tang, Z. Zhao, C. Zhao, Y. Xiang, *Reprod. Biol. Endocrinol.* 19 (2021) 178.
- [80] A. Tivey, M. Church, D. Rothwell, C. Dive, N. Cook, *Nat. Rev. Clin. Oncol.* 19 (2022) 600.
- [81] L.-P. Jia, R.-J. Zhao, Z. Feng, M.-Y. Wang, R.-N. Ma, W.-L. Jia, L. Shang, W. Zhang, Q.-W. Xue, H.-S. Wang, *Sensor. Actuator. B Chem.* 350 (2022), 130849.
- [82] W. Zhang, Z. Dai, X. Liu, J. Yang, *Biosens. Bioelectron.* 105 (2018) 116.
- [83] Y. Huang, M. Tao, S. Luo, Y. Zhang, B. Situ, X. Ye, P. Chen, X. Jiang, Q. Wang, L. Zheng, *Anal. Chim. Acta* 1107 (2020) 40.
- [84] L. Guo, Z. Mu, B. Yan, J. Wang, J. Zhou, L. Bai, *Sensor. Actuator. B Chem.* 350 (2022), 130874.
- [85] H. Chai, P. Miao, *Chin. Chem. Lett.* 32 (2021) 783.
- [86] S.M. Kim, J. Kim, G. Yim, H.J. Ahn, M. Lee, T.-H. Kim, C. Park, J. Min, H. Jang, T. Lee, *Anal. Bioanal. Chem.* 414 (2022) 3197.
- [87] K. Fan, R. Yang, Y. Zhao, C. Zang, X. Miao, B. Qu, L. Lu, *Sensor. Actuator. B Chem.* 321 (2020), 128515.
- [88] Q.U.A. Zahra, Z. Luo, R. Ali, M.I. Khan, F. Li, B. Qiu, *Nanomaterials* 11 (2021) 840.
- [89] Z. Wu, H. Zhou, Q. Han, X. Lin, D. Han, X. Li, *Analyst* 145 (2020) 4664.
- [90] M.I. Hutchings, A.W. Truman, B. Wilkinson, *Curr. Opin. Microbiol.* 51 (2019) 72.
- [91] M.A. Blunston, A. Yonovitz, E.L. Woodahl, M.H. Smolensky, *Chronobiol. Int.* 32 (2015) 1223.
- [92] M.C. Morales-Alvarez, *Adv. Chron. Kidney Dis.* 27 (2020) 31.
- [93] L.P. Rybak, V. Ramkumar, D. Mukherjea, *Front. Neurol.* 12 (2021).
- [94] X. Fu, P. Wan, P. Li, J. Wang, S. Guo, Y. Zhang, Y. An, C. Ye, Z. Liu, J. Gao, J. Yang, J. Fan, R. Chai, *Front. Cell. Neurosci.* 15 (2021).
- [95] Z. Khajavian, M. Esmaelpourfarkhani, M. Ramezani, M. Aliboland, K. Abnous, S.M. Taghdisi, *Microchem. J.* 160 (2021), 105657.
- [96] P. Tavakoli, S.M. Taghdisi, P. Maghami, K. Abnous, *Spectrochim. Acta Mol. Biomol. Spectrosc.* 267 (2022), 120626.
- [97] C.-C. Chang, C.-F. Li, Z.-H. Yang, P.-Y. Lin, H.-C. Chang, C.-W. Yang, *Sensor. Actuator. B Chem.* 364 (2022), 131823.
- [98] G. Zheng, L. Zhao, D. Yuan, J. Li, G. Yang, D. Song, H. Miao, L. Shu, X. Mo, X. Xu, L. Li, X. Song, Y. Zhao, *Biosens. Bioelectron.* 198 (2022), 113827.
- [99] J. Chen, B. Guo, X. Liu, J. Zhang, J. Zhang, Y. Fang, S. Zhu, B. Wei, Y. Cao, L. Zhan, *Exp. Hematol. Oncol.* 11 (2022) 98.
- [100] X. Jiang, B. Liu, Z. Nie, L. Duan, Q. Xiong, Z. Jin, C. Yang, Y. Chen, *Signal Transduct. Targeted Ther.* 6 (2021) 74.
- [101] H.-Y. Q. Pu, Z. Weng, X. Zhou, J. Li, Y. Yang, W. Luo, Y. Guo, H. Chen, D. Wang, G. Xie, *Biosens. Bioelectron.* 194 (2021), 113625.
- [102] L. Guo, B. Lu, Q. Dong, Y. Tang, Y. Du, B. Li, *Anal. Chim. Acta* 1106 (2020) 191.
- [103] X. Chen, Y. Deng, G. Cao, Y. Xiong, D. Huo, C. Hou, *Chem. Commun.* 57 (2021) 6129.
- [104] Y. Deng, G. Cao, X. Chen, M. Yang, D. Huo, C. Hou, *Talanta* 232 (2021), 122415.
- [105] X. Chen, X. Wang, Z. Lu, H. Luo, L. Dong, Z. Ji, F. Xu, D. Huo, C. Hou, *Sensor. Actuator. B Chem.* 311 (2020), 127898.
- [106] L.-r. Zhang, G. Zhu, C.-y. Zhang, *Anal. Chem.* 86 (2014) 6703.
- [107] Y. Liu, S. Zhou, H. Sun, J. Dong, L. Deng, N. Qi, Y. Wang, D. Huo, C. Hou, *Anal. Chim. Acta* 1215 (2022), 339973.
- [108] G. Tian, D. Zhang, Y. Wang, T. Hu, Y. Lin, Y. Wang, W. Cheng, Q. Xia, *Anal. Chim. Acta* 1176 (2021), 338755.
- [109] F. Shen, H. Qian, Y. Cheng, Y. Xie, H. Yu, W. Yao, R. Pei, Y. Guo, H.-W. Li, *Talanta* 206 (2020), 120216.
- [110] T.J. Liang, *Hepatology* 49 (2009) S13.
- [111] M.A. Croxen, B.B. Finlay, *Nat. Rev. Microbiol.* 8 (2010) 26.
- [112] B. Hu, H. Guo, P. Zhou, Z.-L. Shi, *Nat. Rev. Microbiol.* 19 (2021) 141.
- [113] J.H. Kim, S. Kim, S.H. Hwang, T.H. Yoon, J.S. Park, E.S. Lee, J. Woo, K.S. Park, *Sensors* 21 (2021) 4132.
- [114] M.A. Reed, Y.V. Gerasimova, *Front. Chem.* 10 (2022).
- [115] B.S. VarnBuhler, J. Moon, S.K. Dey, J. Wu, S.R. Jaffrey, *ACS Chem. Biol.* 17 (2022) 840.
- [116] J. Yu, J. Liu, C.-B. Ma, L. Qi, Y. Du, X. Hu, Y. Jiang, M. Zhou, E. Wang, *Anal. Chem.* 94 (2022) 600.
- [117] W. Feng, W. Zong, F. Wang, S. Ju, *Mol. Cancer* 19 (2020) 100.
- [118] Z. Duma, A.A. Chuturgoon, V. Ramsuran, V. Edward, P. Naidoo, M.N. Mpaka-Mbatha, K.N. Bhengu, N. Nembe, R. Pillay, R. Singh, Z.L. Mkhize-Kwitshana, *Glob. Health* 18 (2022) 5.
- [119] C.-C. Lai, T.-P. Shih, W.-C. Ko, H.-J. Tang, P.-R. Hsueh, *Int. J. Antimicrob. Agents* 55 (2020), 105924.
- [120] G. Han, Q. Lin, J. Yi, Q. Lyu, Q. Ma, L. Qiao, *Talanta* 242 (2022), 123297.
- [121] A.M. Zaki, S. van Boheemen, T.M. Bestebroer, A.D.M.E. Osterhaus, R.A.M. Fouchier, *N. Engl. J. Med.* 367 (2012) 1814.
- [122] A. Zumla, D.S. Hui, S. Perlman, *Lancet* 386 (2015) 995.
- [123] G. Kim, J. Kim, S.M. Kim, T. Kato, J. Yoon, S. Noh, E.Y. Park, C. Park, T. Lee, J.-W. Choi, *Sensor. Actuator. B Chem.* 352 (2022), 131060.
- [124] T. Yu, H. Xu, Y. Zhao, Y. Han, Y. Zhang, J. Zhang, C. Xu, W. Wang, Q. Guo, J. Ge, *Sci. Rep.* 10 (2020) 9190.
- [125] J.D. Moon, J. Wu, S.K. Dey, J.L. Litke, X. Li, H. Kim, S.R. Jaffrey, *Cell Chem. Biol.* 28 (2021) 1569.
- [126] J. Liu, Y. Zhang, H. Xie, L. Zhao, L. Zheng, H. Ye, *Small* 15 (2019), 1902989.
- [127] J. Zhou, Q. Lin, Z. Huang, H. Xiong, B. Yang, H. Chen, J. Kong, *Anal. Chem.* 94 (2022) 5723.
- [128] H. Ravan, A. Norouzi, N. Sanadgol, E. Hosseinzadeh, *Microchim. Acta* 187 (2020) 392.
- [129] Y. Ou, X. Jin, J. Fang, Y. Tian, N. Zhou, *Microchem. J.* 156 (2020), 104823.
- [130] Z. Khoshbin, K. Abnous, S.M. Taghdisi, A. Verdian, *TrAC, Trends Anal. Chem.* 142 (2021), 116325.